Applied Catalysis B: Environmental 92 (2009) 41–49

Contents lists available at ScienceDirect

Applied Catalysis B: Environmental

journal homepage: www.elsevier.com/locate/apcatb

Photoeletrochemical generation of hydrogen over carbon-doped TiO_2 photoanode

Bin Zhou [a,b,c], Meghan Schulz [d], H.Y. Lin [a], S. Ismat Shah [d,e], Jiuhui Qu [b], C.P. Huang [a,*]

[a] Department of Civil and Environmental Engineering, University of Delaware, 352 Du Pont Hall, Newark, DE 19716, USA
[b] Research Center of Eco-Environmental Sciences, Chinese Academy of Science, Beijing 100085, China
[c] Graduate School, Chinese Academy of Science, Beijing 100039, China
[d] Department of Material Sciences and Engineering, University of Delaware, Newark, DE 19716, USA
[e] Department of Physics and Astronomy, University of Delaware, Newark, DE 19716, USA

ARTICLE INFO

Article history:
Received 20 April 2009
Received in revised form 20 July 2009
Accepted 23 July 2009
Available online 3 August 2009

Keywords:
C-TiO_2
Hydrogen generation
Photoelectrochemical process
Sacrificial reagents

ABSTRACT

Nanostructured carbon-doped TiO_2 (C-TiO_2) thin film was prepared by pulsed laser deposition (PLD) on ITO substrate. Results of X-ray diffraction (XRD) analysis of the thin film showed that the crystal structure of the C-TiO_2 was a hybrid of rutile and anatase. Data of X-ray photoelectron spectroscopic (XPS) analysis confirmed the successful incorporation of carbon into TiO_2 molecules, which formed defects. These defects narrowed the band gap of the C-TiO_2 from 3.25 eV of pure TiO_2 to 3.15 eV. The photoelectrochemical property of the C-TiO_2 film was examined by evaluating the efficiency of hydrogen generation by water splitting in a two-compartment electrochemical system. The fastest rate of gas production was obtained when the thin film was irradiated by light at a wavelength of 325 nm; the photoresponse under visible radiation was limited, however. Applying a bias potential across the photoanode and its counter electrode can increase hydrogen generation effectively. Organic substance added to the photoanodic chamber was photocatalytically degraded which increased the photocurrent and subsequently enhanced hydrogen generation.

1. Introduction

Hydrogen is emerging as the favorite alternative energy over fossil fuels due to its high heating value and small environmental footprint. The commonly used methods for hydrogen generation include chemical reduction [1], biological reduction [2], electrolysis [3], or thermolysis [4]. The chemical method of reforming hydrocarbons while producing hydrogen normally emits carbon dioxide. The microalgae, both eucaryotes and procaryotes are hard to maintain because of their sensitivity to the environmental conditions. Both the electrolysis and thermolysis methods consume substantial amount of energy. Consequently there are needs to find new ways for hydrogen production; especially those techniques that are energy and cost effective.

Since the first discovery by Fujishima and Honda that water can be photoelectrochemically cleaved to H_2 and O_2 using n-type TiO_2 as the anode in 1972 [5], heterogeneous photocatalysis has become a promising method for hydrogen generation so much so that it has attracted world-wide attention. It makes the utilization of free solar energy for hydrogen production possible. Among the various photocatalysts studied for hydrogen production, titanium dioxide (TiO_2) has been proven to be one of the most effective materials because of its attractive photocatalytic activity, photostability, and other advantages such as nontoxicity and low cost [6–8]. But some deficiencies inherently limit the photoactivity of the catalyst. One problem is that the band gap of TiO_2 is so large (3.0–3.2 eV) that only the light with a wavelength shorter than 413–387 nm can be absorbed, which means that only a small portion of the sunlight can be utilized. Another issue is that the photogenerated holes and electrons tend to recombine after photoexcitation to yield a neutral state through emission of photons in a volumetric or surface level. Doping a TiO_2 catalyst, particularly with nonmetallic elements, introduces trapping sites, prevents the rapid recombination of holes and electrons, and improves the catalytic activity. The trapping of electrons effectively increases the lifetime of holes. Non-metallic elements such as nitrogen [9,10], carbon [11,12], sulfur [13], boron [14], and fluorine [15] have been used to impregnate the structure of TiO_2. It was found that the substitutional carbon dopant incorporated into TiO_2 drastically affected the electronic structure of the material and hence improved its photoactivity due to significant overlap between O $2s^2$ $2p^4$ and the carbon states near the valence band edge [16]. Different interpretations of the nature of the carbon doping species have also been proposed. For example, carbonate species has been suggested [17]. The valence shell of the C atom contains four electrons ($2s^2$ $2p^2$), as does the Ti atom ($4s^2$ $3d^2$), but can also host up to four excess electrons, as is formally the case in TiC. In any way, high efficiency in water splitting to hydrogen has been reported using C-TiO_2 [18,20,21].

* Corresponding author. Tel.: +1 302 831 8428.
E-mail address: huang@ce.udel.edu (C.P. Huang).

0926-3373/$ – see front matter © 2009 Elsevier B.V. All rights reserved.
doi:10.1016/j.apcatb.2009.07.026

Several depositing techniques to prepare carbon-doped TiO_2 thin films have been reported. Khan et al. [18] prepared carbon-doped rutile TiO_2 by oxidizing titanium sheet in natural gas flame and obtained water-splitting efficiency of 8.35% with a visible light absorption shifted from 414 to 535 nm. Noworyta and Augustynski [19] used hydrocarbon-flame-oxidation method to prepare C-TiO_2. The spectral photoresponses shifted from 400 to 425 nm. Xu and Khan synthesized carbon modified thin films by spray pyrolysis [20] and by calcination of Ti sheet in air followed by oxidation in natural gas [21]. They reported an enhancement of water splitting rate by visible light irradiation. However, there were questions raised with the results of Khan et al. [18] and Xu et al. [20,21]. Hagglund et al. [22] pointed out that an efficiency of 8.35% reported by Khan et al. was even higher than the theoretical value of 8.1% and that Khan et al. did not compensate for the different spectral photon flux distribution when comparing the overall intensity of the experimental light source with that of standard solar illumination. Furthermore, Murphy [23] thought that Khan et al. underestimated the bias voltage, thereby underestimating the irradiation while converting the light source of xenon arc lamp to the AM 1.5 global solar spectrum as mentioned by Hagglund. Neumann et al. [24] prepared photoelectrode by the hydrolysis of titanium tetrachloride with carbon-containing bases. However, the prepared film had no obvious spectrum extension to the visible light. Enache et al. [25] used spray pyrolysis of organometallic precursor in CO_2/O_2 atmosphere for the fabrication of C-TiO_2 film and reported that no photocurrent was detected under the irradiation of visible light. Zhu et al. [26] studied the photoelectrochemical response of carbon-doped TiO_2 thin film obtained by DC reactive magnetron sputtering. The band gap of the films decreased from 3.2 (pure TiO_2) to 3.1 eV when the molar ratio of C to Ti was 0.05 in the target. Further when the ratio was increased to 0.10 the thin film expressed the highest photocurrent density of 0.069 $\mu A\,cm^{-2}$ at 0 V (without bias potential) under visible light illumination.

As far as we know, there is no report about the fabrication of carbon-doped TiO_2 thin film by PLD method. Pulsed laser deposition is a high-energy process. It has numerous advantages over conventional deposition methods. PLD ensures a well adherent thin film with good mechanical rigidity [27] and surfaces with high specific surface area [28]. In addition, PLD also offers advantages such as stoichiometrically transferring material from target to substrate, capability of depositing both inert and reactive gases, wide range of operational pressure and temperature, and broad selection in substrate materials.

Besides the technique employed for fabricating novel thin film photoelectrode, another approach that can decrease effectively the recombination of hole–electron pairs is to apply a bias potential to the photocatalyst while it is being irradiated by light, which is called photoelectrochemical (PEC) process [29,30]. In a photoelectrochemical system, the photocatalyst is deposited on an electrode externally connected to, normally, a metal electrode. The photogenerated holes oxidize and decompose the target substance at the surface of the photoanode. Meanwhile, the photogenerated electrons move through the external circuit to the counter electrode driven by the externally applied electrical force. The electrons only cannot reduce hydronium ions or water molecules to produce hydrogen molecules. For spontaneous water splitting process, the voltage between the working and the counter electrode should be no less than 1.23 V (pH = 0). Rutile TiO_2 can generate photovoltage of only 0.7–0.9 V under solar light illumination [31]. Therefore a proper external bias potential is also needed to raise the energy level above the electrochemical potential of the half-reaction for hydrogen generation. And in that case, the hydrogen evolution and oxidation of target substance can be carried out on the cathode and anode separately at the same time.

In this study, nanostructured carbon-doped TiO_2 was successfully immobilized onto quartz substrate coated with indium-doped tin oxide (ITO) by pulsed laser deposition. The surface topography, crystalline structure, binding energy, and photocurrent onset of the thin film were characterized. Its photoelectrochemical property was measured by hydrogen generation with or without sacrificial agents. Furthermore, the degradation of 2,4-dichlorophenol (2,4-DCP) under monochromatic light irradiation was conducted in a two-compartment PEC system.

2. Experimental

2.1. Preparation of C-TiO_2 thin film

The C-TiO_2 thin film was prepared via laser ablation of a pure (99.999%, Sigma–Aldrich) TiO_2 target with a KrF gas excimer laser (Lambda Physik LPX 305, λ = 248 nm) on ITO glass under a partial methane atmosphere. Base pressure in the chamber was maintained below 0.01 Pa with a turbo molecular pump and a mechanical pump. The chamber was kept at 13.3 Pa during deposition, with 6.7 Pa of CH_4 and 50 Pa of O_2/Ar buffer gas. The ITO-coated glass substrates were kept stationary and heated to 600 °C via irradiative 500-W halogen lamps, while the target was being rotated at ~15 rpm and at an angle of 45° with respect to the incident laser. The energy output and frequency of the laser pulse was set to 0.45 J and 15 Hz, respectively. After deposition for 20 min, it gave the film a thickness of approximately 1.5 μm, or 0.08 μm/pulse. Prior to deposition, the ITO glass substrate was cleaned ultrasonically in pure acetone solution and triple-rinsed with deionized water.

2.2. Sample characterization

X-ray diffraction patterns (XRD) were gathered using a Rigaku D-Max B diffraction system, with a Cu Kα radiation source (1.5405 Å) and graphite crystal monochromator. Survey scans from $2\theta = 20°$ to 80° were performed with a step size of 0.05°. Regional high-resolution XRD spectra were also obtained to investigate TiO_2 lattice parameters, using step size of 0.002°. X-ray photoelectron spectroscopy (XPS) was performed to evaluate surface composition and structure, using a SSI-M probes XPS system with Al Kα radiation source ($h\nu$ = 1486.6 eV). Survey scans were performed at Δ = 0.25 eV, with higher resolution scans of the carbon, titanium, and oxygen regions at Δ = 0.05 eV. Surface images came from a JEOL scanning electron microscope (model JSM 7400F) for analyzing the topography of prepared films. Working distance was kept between 7.4 and 7.7 mm and accelerating voltage was 2–3 kV. General absorption spectra were obtained using a double-beam Lambda 35 Perkin-Elmer UV-Vis spectrophotometer with a $BaSO_4$ integrating sphere.

2.3. Photoelectrocatalytic experiments

The photoelectrocatalytic activities of the C-TiO_2 were evaluated in terms of hydrogen generation, the oxidation of alcohols, and the degradation of 2,4-dichlorophenol (2,4-DCP) under ultraviolet light irradiation at ambient temperature. Photoelectrochemical experiments were carried out in a three-electrode system. The C-TiO_2 thin film was used as the working electrode and a single 6-cm long platinum wire was used as the counter electrode. A saturated calomel electrode (SCE) was selected as the reference electrode. To better evaluate the capability of hydrogen generation and degradation of organic substance by C-TiO_2 thin film, a two-compartment reactor was made to separate the anode

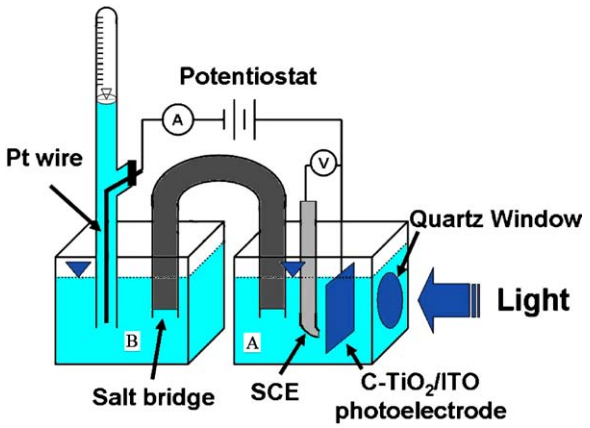

Fig. 1. Schematic diagram of the two-chamber PEC system.

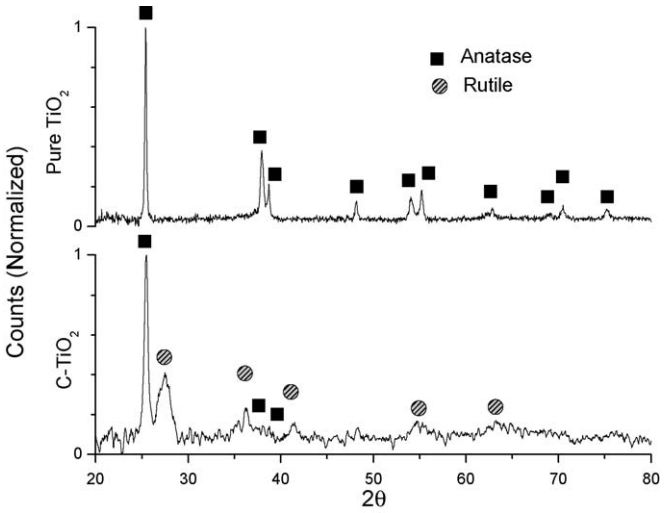

Fig. 2. Normalized XRD spectra of undoped (top) and carbon-doped (bottom) TiO_2 thin films.

and the cathode. These two compartments were connected by a salt bridge. The C-TiO_2 thin film, the anode, was placed with the reference electrode in the photoanodic chamber (A) and the Pt wire as the cathode was in the electrochemical chamber (B). The custom-made reactor was opaque and there was a small window at a size of 1 cm × 1 cm on one side of chamber (A), which was made of optical quality quartz. The light emitted from a monochromatic excitation source (Model RF-5301, Shimadzu, Japan) passed through the window and irradiated directly onto the C-TiO_2 photoelectrode. The band pass of the monochromator is 2 nm. The light intensity at the surface of the photoelectrode was about 7.5 mW/cm^2 when the wavelength of the incoming light was set at 350 nm. Potentiostatic control was maintained with a potentiostat (Model AFRDE 4, Pine Instrument Inc., USA). The solution volume in chamber (A) and chamber (B) were 100 and 80 mL, respectively. Electrolyte was provided with 0.1 M of Na_2SO_4. H_2SO_4 and NaOH solutions were used to adjust the pH value. The gas collected in cathodic chamber was examined by a gas chromatograph (5890 series II, Agilent, USA) for determining the amount of hydrogen produced. Fig. 1 shows the entire setup. 2,4-DCP concentration was analyzed by reversed-phase HPLC with an Agilent 1100 HPLC apparatus. A C-18 column (Agilent ZORBAX Eclipse XDB-C-18) was used. The mobile phase employed was a mixture of 70:30 methanol/water containing 1% acetic acid with flow rate of 1.0 mL min^{-1}. The detective wavelength of the detector was 287 nm.

3. Results and discussion

3.1. Characterization of C-TiO_2 thin film

Fig. 2 shows the X-ray diffraction (XRD) spectra of the C-doped TiO_2 thin film, compared to an undoped film prepared under otherwise same conditions. Deposition at 13.3 Pa O_2/Ar and 600 °C produced a polycrystalline film in the anatase structure. However, introducing CH_4, a carbon-containing gas, changed the anatase structure to a mixture of both anatase and rutile phases. Rutile is the more densely packed and thermodynamically stable phase than anatase, whereas the later is commonly considered the more photoactive form of TiO_2. Di Valentin et al. [17] calculated the density function of the semiconductor and showed that carbon doping of TiO_2 favored the formation of oxygen vacancies, which might enhance the photoactivity. The grain size was approximately 20 nm for both the undoped and C-doped films calculated from the Scherrer equation [27]. Peak positions 2θ were obtained via Voight function fits of high-resolution regional scans. The lattice constants were calculated using the following expression based on the Bragg diffraction theory [32]:

$$d_{hkl} = \frac{\lambda}{2\sin\theta} = \frac{ac}{\sqrt{a^2l^2 + c^2(h^2 + k^2)}} \quad (1)$$

where the rightmost expression stems from the tetragonal character of anatase and rutile ($a = b \neq c$). This equation becomes solvable when one observes a pair of distinct ($h\,k\,l$) reflections. The calculated c/a ratios deviated by less than 0.5% from the literature values of 2.510 [33] for anatase and 0.644 for rutile [34], indicating no significant strain in the lattice with carbon incorporation.

X-ray photoelectron spectroscopy (XPS) was used to examine the chemical composition of C-TiO_2 thin film. Survey scans showed titanium, oxygen, and carbon being the main elements present on the surface of both pure and C-TiO_2. It was expected to see carbon on the undoped sample, as well as any other thin film exposed to air, due to the adsorption of organics and dusts. The small peak near 290 eV in Fig. 3a was typical of CO_2 adsorbed from atmosphere. Traces of nitrogen and fluorine were present at amounts less than two atomic percents. The oxygen and titanium regional scans showed no difference between the doped and the undoped samples; the O 1s peak, located at 531.0 eV, and Δ (Ti 2p1/2 − Ti 2p3/2) = 5.7 eV both agreed well with the literature values [35]. The C 1s peak from graphite was present in both samples, as presented in Fig. 3a. There was also a small peak due to the absorption of inorganic carbon such as CO_2 near 289 eV. Other than superficial signal intensity, we observed no difference in the carbon signal to suggest difference in structure. Based on the above C 1s signal, the carbon content in the prepared C-TiO_2 film was estimated to be about 0.3 % (molar percent).

A detailed scan of the valence band region was also done for the thin film. The valence band of crystalline TiO_2 was composed mainly of O2p states. It has been theorized that carbon doping would increase photoactivity by adding carbon defect states in the forbidden region, overlapping with the O 2p states [16]. The shape of the valence band did change with carbon incorporation. Small increase in states near the valence band edge (6.9 eV) was detected upon carbon incorporation, suggesting additional states near the edge of the valence band (Fig. 3b). This is supported by recent studies in our group on higher C concentrations, in which the trend in valence band augmentation continues [36].

Surface morphology of the thin film was examined by SEM as shown in Fig. 4. Both coatings of pure TiO_2 and C-TiO_2 strongly

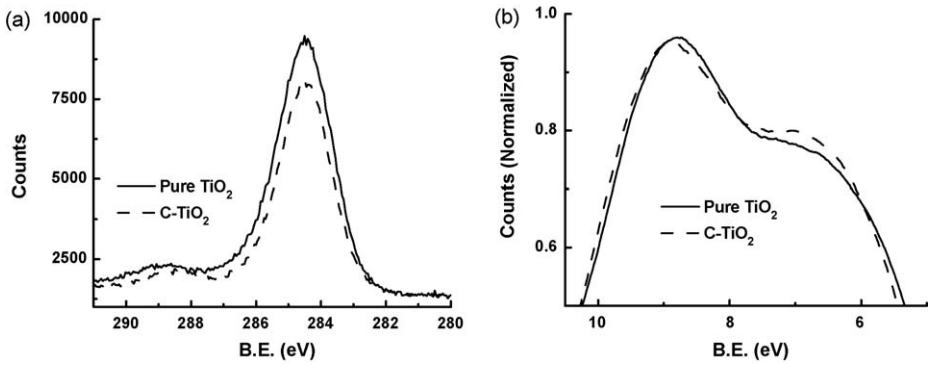

Fig. 3. XPS spectra of C-TiO_2 thin film. (a) Regional scan for C 1s peak; (b) regional scan for the valence band edge.

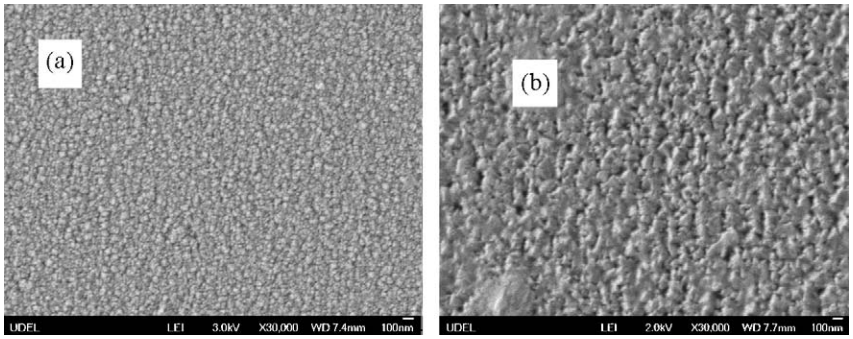

Fig. 4. SEM images of the surface of undoped (a) and carbon-doped (b) TiO_2 thin film.

adhere to the glass surface. The nanocrystallites covered the surface of the substrate evenly, in a shape of compact sphere. There were no pores between catalyst particles. From the SEM images, it can be seen that the size of C-TiO_2 particles was larger than that of pure TiO_2. The size of most of the C-TiO_2 particles was around 100 nm. This result is different from that calculated by the Scherrer equation using the XRD data by a factor of five. It appears that the SEM images reveal the formation of aggregates rather than the individual primary crystals.

The diffuse reflectance spectrum of C-TiO_2 and pure TiO_2 thin film was measured and shown in Fig. 5. The curves reflect the optical absorption property of the semiconductor catalyst. It is relevant to the electronic structure. The corresponding onset adsorption edge for C-TiO_2 was 413 nm, nearly 25 nm red shift compared to pure TiO_2. That means the incorporation of carbon atoms extends the photosensitive region of TiO_2 to the visible range. For semiconductor catalysts, the optical band gap could be estimated by the Kubelka–Munk function as follows [37]:

$$Ah\upsilon = c(h\upsilon - E_g)^n \quad (2)$$

where A is the absorption coefficient; $h\upsilon$ is the photons' energy; c is constant ($c = 1$); E_g is band gap energy. In the above equation, n is a constant which is determined by the type of semiconductor, that is, a direct band gap for $n = 1/2$ and an indirect band gap for $n = 2$.

$(Ah\upsilon)^2 - h\upsilon$ plot was drawn (Fig. 5) using the data and Eq. (2) above. The E_g for C-TiO_2 was 3.15 eV and that for pure TiO_2 was 3.25 eV.

Based on the above results, the band gap reduction of C-TiO_2 might be attributed to the phase change of TiO_2 from anatase to a mixed phase containing both anatase and rutile. Carbon doping plays an insignificant role on the band gap narrowing.

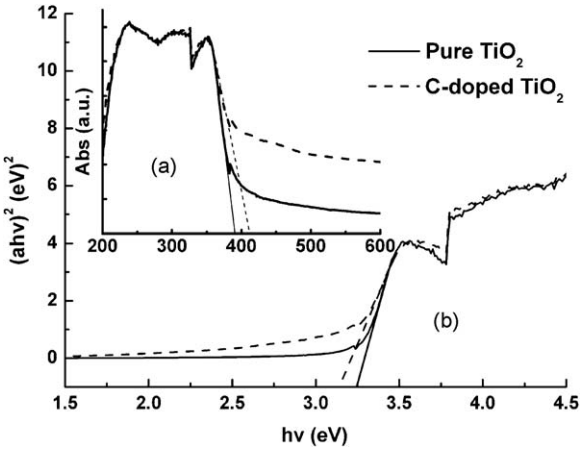

Fig. 5. (a) UV–vis spectra of undoped and carbon-doped TiO_2 thin film; (b) band gap determination of undoped and carbon-doped TiO_2 thin film from the $(Ah\upsilon)^2$ versus $h\upsilon$ plot.

3.2. Evaluation of photoelectrocatalytic activities

Fig. 6 shows the current–potential plots at various wavelengths for the C-TiO_2 and pure TiO_2 thin films in aqueous solutions. The incoming light included both UV light (e.g., 300, 325, 350, and 375 nm) and visible light (e.g., 400 and 425 nm). It is clear that for the C-TiO_2 film, the highest photocurrent response was obtained under the irradiation of 325 nm UV light among all seven-radiation conditions. The photocurrent increased first and then decreased while the wavelength of the incoming light increased. The decrease of photocurrent from 325 to 300 nm was attributed to the decrease of light intensity (Table 1b). The increase in photocurrent is governed by the wavelength; the shorter the wavelength of the incoming light, the higher the energy it is transferred. With higher energy, photons can acquire a greater initial kinetic energy, which facilitates their movement. At a bias potential of 1.00 V, the

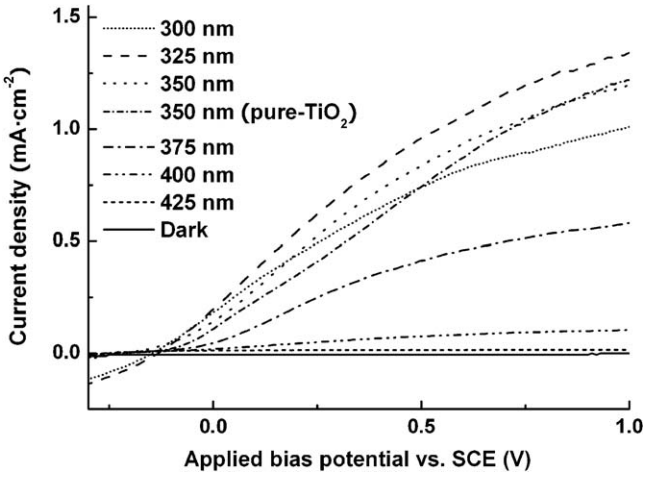

Fig. 6. Current–potential plots for different incident light (wavelength = 300, 325, 350, 375, 400, and 425 nm). Experimental conditions: chamber (A) pH = 11, chamber (B) pH = 2; λ = 350 nm; 0.1 M Na_2SO_4 as electrolyte.

Table 1
Hydrogen generation efficiency and photoconversion efficiency as a function of bias potential (a) and irradiation wavelength (b).

(a)				
V_{bias} vs. SCE (V)	0.25	0.50	0.75	1.00
V_{bias} (working and counter electrode, V)	1.10	1.65	2.08	2.48
Current (I_p, mA)	0.54	0.84	1.05	1.20
Light intensity (P_t, mW/cm^2)	7.5	7.5	7.5	7.5
Current efficiency (%)	84	84	90	95
Photoconversion efficiency (%)	0.4	6.7	14.4	22.9
(b)				
Wavelength (nm)	300	325	350	375
V_{bias} (working and counter electrode, V)	1.87	2.21	2.08	1.54
Current (I_p, mA)	0.89	1.20	1.05	0.51
Light intensity (P_t, mW/cm^2)	4.5	6.2	7.5	8.0
Current efficiency (%)	76	98	90	88
Photoconversion efficiency (%)	16.2	22.4	14.4	3.1

photocurrent generated by UV light at a wavelength of 325 nm was over 12 times that of 400 nm, which is at the beginning of the visible spectrum. When the wavelength of the incoming light was at 425 nm, the photocurrent still could be detected, but was weak. This result is consistent with that reported by Neumann et al. [24], Enache et al. [25], and Zhu et al. [26] that it is difficult to extend the photoresponse to visible light region. The absorbance shifted at least by 12 nm to red than that calculated using the Kubelka–Munk equation. Band gap obtained from diffuse reflectance measurement could be deviated from the true value due to difference in film thickness or the particle size of photocatalysts [38]. It was found that introducing carbon into the lattice of TiO_2 could increase the photocurrent when the bias potential was in the range from 0 to 0.75 V. Results from Fig. 6 also illustrate that external bias potential is a key operational factor in a PEC system. It can be observed simply that higher bias potential generated higher photocurrent. The photocurrent increased significantly as the bias potential increased then remained relatively constant as the bias potential continued to increase. The application of positive potentials across the photoelectrode establishes a potential gradient within the C-TiO_2 film and increases the photocurrent, which produces effect similar to that caused by band bending in single-crystal photoelectrodes [39]. As the positive potential increases, the resulting gradient separates holes and electrons, thereby decreases their recombination. The electron–hole pairs first at or near the surface, then inside of the photoelectrode are separated by the externally applied electric field. At last, the photocurrent increases with the bias potential until most photogenerated electrons are transferred to the cathode under the electric field applied. The bias potential at which the maximum photocurrent takes place is dependent on the conditions during the synthesis of the photoelectrodes [40].

To examine the photocatalytic efficiency of the C-TiO_2 thin film, the incident photon conversion efficiency [IPCE(λ)], also called external current efficiency, was calculated using the data shown in Fig. 6. The [IPCE(λ)] is defined as the number of electrons transferred per incident photon[41]:

$$\text{IPCE}\,(\%) = \frac{J_{sc}(\lambda)}{eI_{inc}(\lambda)} = \left[1240\frac{J_{sc}\,(\text{A/cm}^2)}{e\lambda\,(\text{nm})I_{inc}\,(\text{W/cm}^2)}\right] \times 100 \qquad (3)$$

where $J_{sc}(\lambda)$ is the short-circuit photocurrent density under monochromatic light (A/cm^2), e is the electron charge (C), and $I_{inc}(\lambda)$ is the incident photon flux (W/cm^2). The [IPCE(λ)] is a measurement of quantum efficiency profile of a particular semiconductor photoelectrode as a function of incident wavelength. At a certain photon energy/wavelength, the quantum efficiency represents the energy difference between the local electronic states and the conduction band minimum. If there is no significant change in energy position of the conduction band minimum, the edge of the [IPCE(λ)] spectrum is qualitatively proportional to the density of states for the valance band maximum. Therefore, the onset of the [IPCE(λ)] spectrum is nearly the same as the wavelength of band gap threshold (λ_{bg}) of a particular semiconductor.

As shown in Fig. 7, the IPCE(λ) of C-TiO_2 started to increase near 425 nm, with the lowest energy of 2.92 eV. The maximum quantum efficiency of about 10.6% was obtained at 325 nm when no bias potential was applied. The IPCE value increased with the increasing external potential. The highest value of 50% was achieved under a bias potential of 1.00 V, also at irradiation of 325 nm. The IPCE for pure TiO_2 was calculated under the same irradiation condition and a bias potential of 0.75 V. In contrast to C-TiO_2 whose photocurrent response started at wavelength of 425 nm, the pure TiO_2 film generated photocurrents almost disappeared at 400 nm. (*Note*: Anatase has a band gap of 3.2 eV or 387 nm in wavelength.) In the whole UV range, the IPCE profile of C-TiO_2 and pure TiO_2 was almost overlapping. It must be noted that the IPCE(λ) function considers the effect of surface morphology and mass transfer limitation on the determination of band gap, whereas the Kubelka–Munk, the UV–vis diffuse reflectance absorption, does not, the band gap obtained from both methods was close.

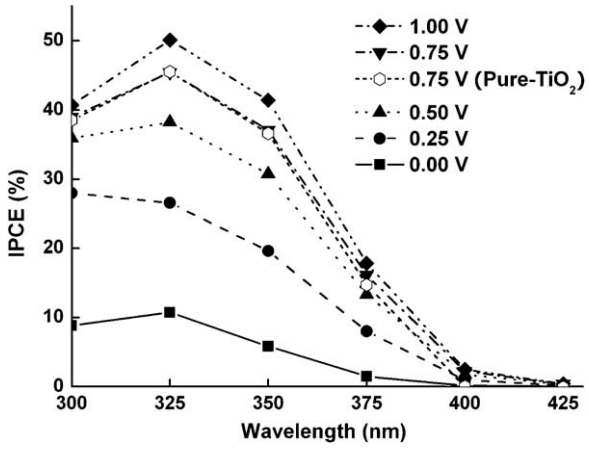

Fig. 7. Plots of incident photo to current conversion efficiency (IPCE) versus wavelength between 300 and 425 nm as a function of bias potential in 0.1 M of Na_2SO_4 electrolyte.

Fig. 8 shows the results of hydrogen generation for the C-TiO_2/ITO electrode at different external bias potentials (Fig. 8a) and irradiation conditions (Fig. 8b). The gas production was a function of the applied potential or illumination. The system with a higher bias potential or an irradiation of shorter wavelength has a faster hydrogen yield. The hydrogen production rate was positively proportionally to the intensity of the photocurrent. The photocurrent provides electrons at the cathode for hydrogen ion reduction. For semiconductor, C-TiO_2 with a band gap of 3.15 eV, it is almost impossible to generate hydrogen just under the irradiation considering the redox potential of H^+/H_2. Bias potential is necessary to initiate this reaction. Fujishima and Honda [5] conducted photoelectrolysis of water and showed that the photovoltage in the cell was not sufficient for water photolysis; an additional bias voltage of 0.25–0.50 V was required. In our experiment, it seemed that 0.25 V was the minimum value. The hydrogen generation rate at the beginning of the photochemical reaction was a small. It increased as the reaction time increased and finally reached a constant value. This observation could be related to the experimental set-up. At the onset of the reaction, the newly generated gas bubbles became attached at the surface of the platinum wire with no gas collection in the manometer. As reaction continued, the hydrogen molecules kept emerging at the cathode surface where the new and the old gas bubbles became agglomerated, grew in size and eventually moved up in the collector when gas detection was possible.

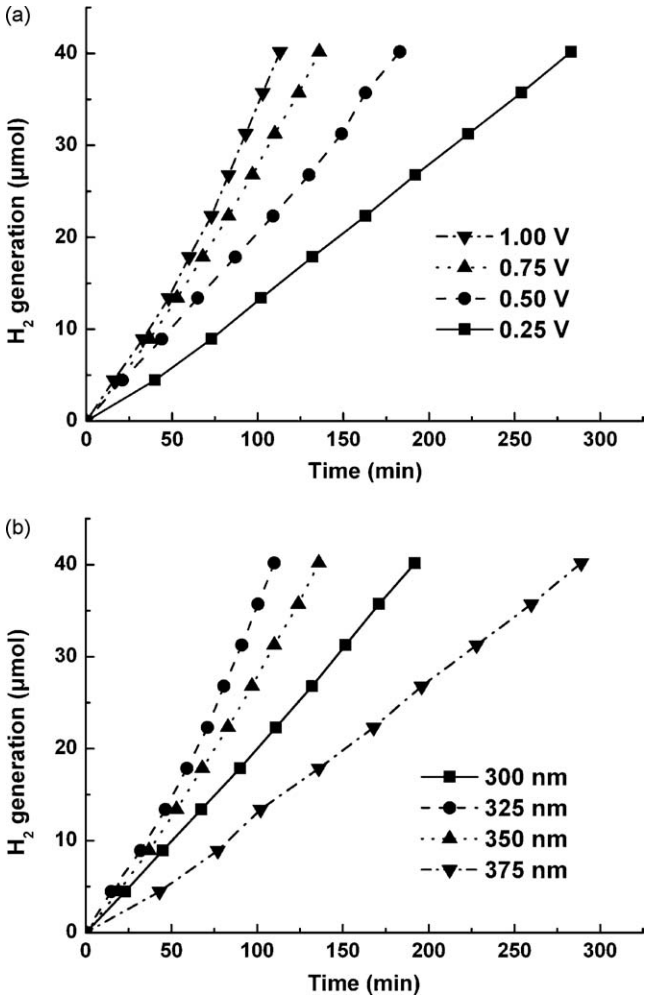

Fig. 8. (a) Influence of applied bias potential on H_2 generation using C-TiO_2 as the photoanode in a PEC system. Experimental conditions: chamber (A) pH = 11, chamber (B) pH = 2; λ = 350 nm; 0.1 M Na_2SO_4 as electrolyte. (b) Influence of the wavelength of the irradiation light on H_2 generation using C-TiO_2 as the photoanode in a PEC system. Experimental conditions: chamber (A) pH = 11, chamber (B) pH = 2; E = 0.75 V; 0.1 M Na_2SO_4 as electrolyte.

Based on the data above, the current efficiency for hydrogen production can be calculated [42]:

$$\mathrm{CE}\,(\%) = \frac{\text{number of molecules produced } (H_2)}{\text{number of electrons flowed}} \times 2 \times 100 \quad (4)$$

The overall photoconversion efficiency is defined as the ratio of the maximum hydrogen production to the total light energy input. The total photoconversion efficiency can be calculated by measuring the bias potentials between the working and the counter electrode, V_{bias}, the photocurrent, I_p, and the power input, P_t, individually according to the following equation upon correction for pH effect, e.g., pH = 2 in this study [43]:

$$\varepsilon_0 = \frac{(1.05 - V_{bias})I_p}{P_t} \quad (5)$$

Table 1a illustrates the results of the calculated current efficiency and photoconversion efficiency at different bias potentials versus SCE under irradiation of UV light at 350 nm. From Table 1a, it can be seen that both the current efficiency and the photoconversion efficiency increased with the increase in bias potential. The highest current efficiency was 95% at bias potential of 1.00 V versus SCE whereas the lowest current efficiency was 84% at bias potential of 0.5 V versus SCE. The photoconversion efficiency reached the highest value of 22.8%. When the bias potential was 0.25 V versus SCE, the potential difference between the photoanode and the counter electrode (cathode) was 1.10 V. Under this condition, the photoconversion efficiency was almost zero. Table 1b shows the current efficiency and the photoconversion efficiency under various wavelengths at a bias potential of 0.75 V versus SCE. The highest current efficiency and photoconversion efficiency were 98% and 22.4%, respectively and occurred at 325 nm.

The experience learned to date has shown that water cleavage is a rather low-efficiency process, whereas the cleavage of some organic substances, such as alcohols, is much efficient for hydrogen production. Additives with ability to donate the lone-pair electron are termed sacrificial reagents that can enhance hydrogen yield. A list of alcohols, namely, methanol, ethanol, and iso-propanol were selected and added to chamber (A) as sacrificial reagents at concentration of 0.15 mol L^{-1}. The results were illustrated in Fig. 9. In general, the presence of sacrificial reagents significantly increased the photocurrent. The system with ethanol had the highest hydrogen production followed by methanol then iso-propanol being the lowest, whatever insignificance expressed

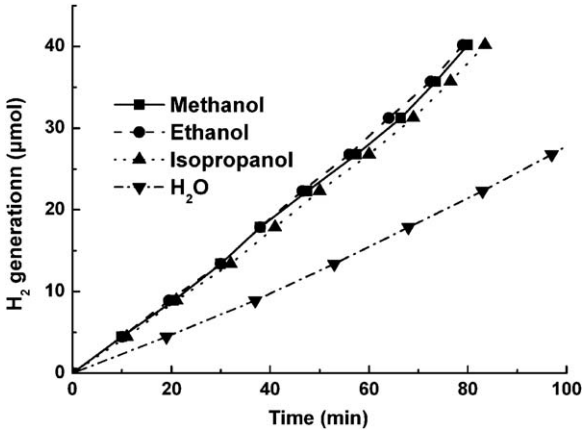

Fig. 9. Influence of sacrificial agents (e.g., alcohols) on H_2 generation using C-TiO_2 as the photoanode in a PEC system. Experimental conditions: chamber (A) pH = 11, chamber (B) pH = 2; λ = 350 nm; E = 0.75 V; 0.1 M Na_2SO_4 as electrolyte.

among them. The efficiency of hydrogen production would be increased when substances were closely adsorbed at the surface of the catalyst. The attached organic compounds promptly would react with photogenerated holes and be oxidized to radical species or other intermediates until they were fully mineralized. Therefore, adsorption process happened at the surface of the photocatalyst would affect in part the strength of photocurrent. It has been reported that solvent polarity would affect the dissociative adsorption of the alcohol over a pair of Ti and O, considered as the controlling step of the photoreaction [44]. Yang et al. studied the effect of monohydric alcohols on photoelectrochemical generation of hydrogen from water and reported that the generation rate followed the decreasing order: methanol > ethanol > iso-propanol [43]. These authors suggested that dipole moment holds key to the efficiency of hydrogen generation; the dipole moment of methanol, ethanol, and iso-propanol was 1.70, 1.69 and 1.66, respectively. Note that the dipole moment of these three alcohols was very close.

Methanol, ethanol, and iso-propanol have, respectively, five-, six-, and six-membered ring structure with a methyl substituent upon adsorption on the C-TiO_2 nanoparticles. Comprehensively considering the solvent polarity, spatial structure and ring stability and based on our results, the affinity of these three alcohols toward C-TiO_2 nanoparticles would follow the order: ethanol > methanol > iso-propanol.

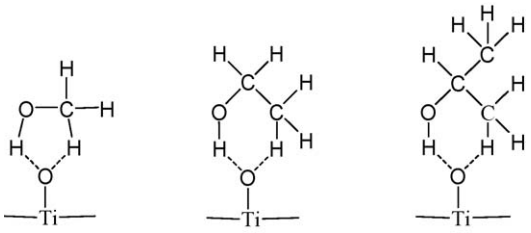

In an aqueous system, the main reactions occurred at the anode were as follows:

$$c - TiO_2 \xleftrightarrow{h\nu} h^+ + e^-_{cb} \quad (6)$$

$$h^+ + H_2O \rightarrow \cdot OH + H^+ + e^- \quad (7)$$

It is well known that the following reaction takes place at the cathode with the generation of hydrogen:

$$2H_2O + 2e^- \rightarrow H_2 + 2OH^- \quad (8)$$

At the anode surface, different reactions could take place dependent on the composition of the electrolyte while the cathode simply splits the water into hydrogen. In aqueous system with the presence of alcohols, some other reactions take place in addition to the above reactions, i.e., (6) and (7).

$$h^+ + RCH_2OH \rightarrow RCOOH + H^+ + e^- \quad (9)$$

$$2^{\bullet}OH + RCH_2OH \rightarrow RCHO + 2H_2O + 2e^- \quad (10)$$

According to reactions (9) and (10), more electrons would be generated when alcohols were present in the electrolyte and these electrons would be transferred rapidly to the cathode together with the photogenerated electrons through the circuit driven by the external bias potential for hydrogen production.

Fig. 10 shows the cyclic voltammetry scans of C-TiO_2/ITO thin film in sodium sulfate electrolyte with and without ethanol. A significant increase in anodic current was observed when 0.015 mol L^{-1} of ethanol was added into the electrolyte. The current kept increasing when the ethanol concentrations were 10 and 100 times that of the initial value, that is, 0.15 and 1.5 M, individually. However, the increment became smaller when the

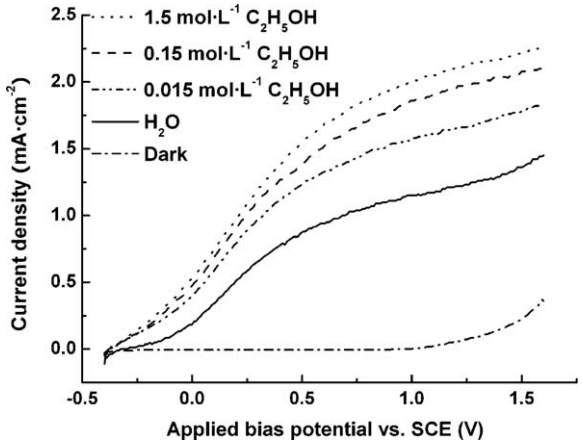

Fig. 10. Current–potential plots for different concentrations of ethanol. Experimental conditions: chamber (A) pH = 11, chamber (B) pH = 2; λ = 350 nm; E = 0.75 V; 0.1 M Na_2SO_4 as electrolyte.

ethanol concentration increased from 0.15 to 1.5 mol L^{-1}. The changes of intensity of the photocurrent were also reflected in the hydrogen production. Fig. 11 shows the relationship between the initial ethanol concentration in chamber (A) and hydrogen production. The rate of hydrogen generation was affected by the ethanol concentration in the reaction mixture. Hydrogen was increased by 28% when ethanol concentration was increased from 0.015 to 0.15 M. Further increase in ethanol concentration from 0.15 to 1.5 M only resulted in a 3% increase in hydrogen production. The generation of valence band holes on the surface of the photocatalyst at sufficient amount required for reacting with ethanol molecules did not increase as long as light intensity, voltage applied, and contact area of the catalyst remained unchanged. The presence of ethanol would only take up the active sites formerly occupied by H_2O on the photoanode surface. When present at high concentrations, such as 1.5 M, the sites available for water molecules are small which leads to insignificant increase in hydrogen production.

It must be mentioned that alcohols are bio-derived organic substances and can be directly used as fuel. In this study, we selected 2,4-dichlorophenol (2,4-DCP) an endocrine disruptor as a sacrificial agent in replacement of the alcohols. Since the concentration of most endocrine disruptors in the environment was much less than that of the ethanol studied, in order to mimic

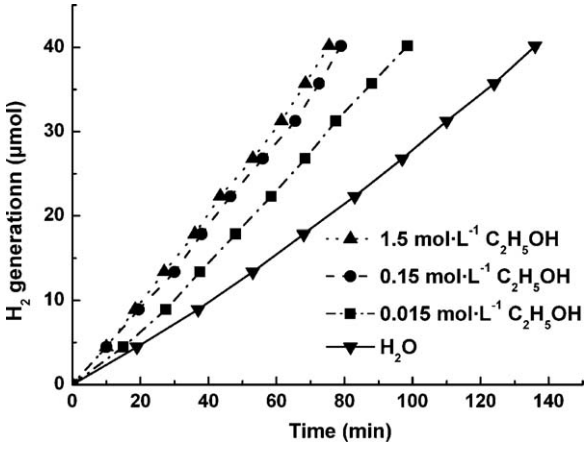

Fig. 11. Influence of concentration of ethanol on H_2 generation using C-TiO_2 as the photoanode in a PEC system. Experimental conditions: chamber (A) pH = 11, chamber (B) pH = 2; λ = 350 nm; E = 0.75 V; 0.1 M Na_2SO_4 as electrolyte.

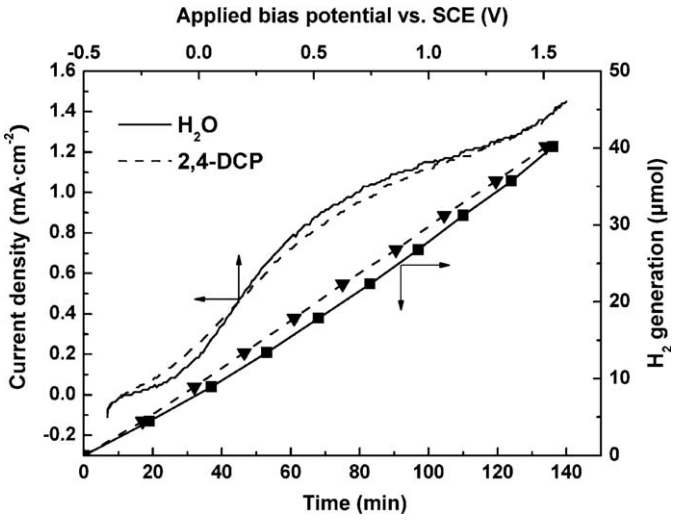

Fig. 12. Effect of 2,4-DCP on photocurrent and H_2 generation. Experimental conditions: chamber (A) pH = 11, chamber (B) pH = 2; λ = 350 nm; E = 0.75 V; 0.1 M Na_2SO_4 as electrolyte.

the natural condition, a 2,4-DCP concentration of 0.06 mM was used. Fig. 12 shows that the photocurrent increased slightly over that of the background electrolyte, i.e., in the absence of 2,4-DCP. The time for producing the same amount of hydrogen was also decreased slightly. The results indicated that the mechanism of anodic radical production (•OH) and subsequent oxidation of the organic substance was operative in the system containing 2,4-DCP. The presence of 2,4-DCP did not have negative impact on photocurrent but promote the hydrogen generation efficiency. Fig. 13 shows the decrease in 2,4-DCP concentrations as a function of time. Results indicated that nearly 50% of 2,4-DCP was degraded in 150 min. This means that simultaneously the degradation of hazardous compounds and hydrogen production can be achieved in the anodic and the cathodic chambers, respectively. Results in Fig. 13 also show the influence of applied external bias potential on the decomposition of 2,4-DCP. The highest extent of 2,4-DCP degradation of about 55% was achieved when a bias potential of 1.00 V was applied. When no bias potential was applied, there was still a 10% decrease in 2,4-DCP concentrations in 150 min, which was only one-fifth of the highest degradation percentage.

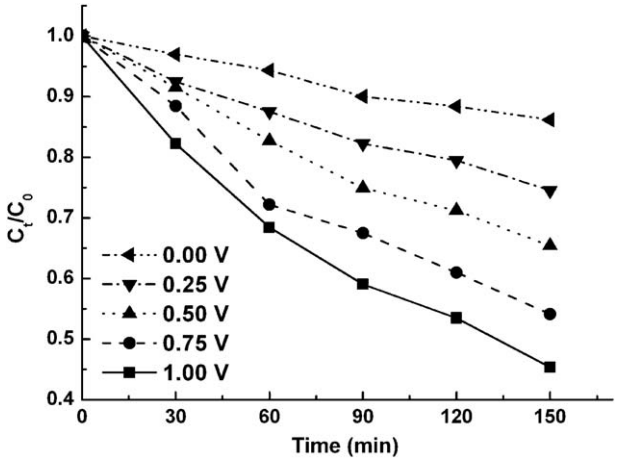

Fig. 13. Effect of bias potential on the degradation of 2,4-DCP using C-TiO_2 as the photoanode in a PEC system. Experimental conditions: [2,4-DCP] = 0.06 mM; chamber (A) pH = 11, chamber (B) pH = 2; λ = 350 nm; 0.1 M Na_2SO_4 as electrolyte.

4. Conclusion

Nanocrystalline carbon-doped TiO_2 thin film was successfully coated onto the substrate of ITO glass via pulsed laser deposition method at 600 °C. XPS data confirmed the incorporation of carbon into the structure by a detailed scan of the valence band region. Oxygen sites in the TiO_2 lattice were substituted by carbon atoms. The introduction of carbon changed the crystal structure of TiO_2 to a mixture of anatase and rutile phases, instead of anatase with pure TiO_2 according to the XRD results. Band gap was successfully narrowed to 3.15 eV, which based on the UV–vis data. The extension of photoreponse to visible wavelength range was limited. It is mainly because the appearance of mixed phases rather than the carbon doping. As to the photoelectrochemical property of the C-TiO_2 thin film, the photocurrent increased with the increase of external bias potential and had the highest value under irradiation of light with a wavelength of 325 nm. The presence of alcohol in electrolyte solution (anodic chamber), especially ethanol significantly enhanced the photocurrent. Photocurrent had a positive relation to the concentration of ethanol. In addition to ethanol, 2,4-DCP could also promote the hydrogen production efficiency. The two-chamber PEC system is capable of hydrogen generation and degradation of hazardous chemicals simultaneously.

Acknowledgements

This work was support by a grant from Federal Administration Transit Grant No. DE-55-7001-00. We wish to thank our unanimous reviewers for their highly professional and constructive comments.

References

[1] J.N. Armor, Appl. Catal. A: Gen. 176 (1999) 159–176.
[2] D. Das, T.N. Veziroglu, Int. J. Hydrogen Energy 26 (2001) 13–28.
[3] D.L. Stojic, M.P. Marceta, S.P. Sovilj, S.S. Miljanic, J. Power Sources 118 (2003) 315–319.
[4] W. Weirich, K.F. Knoche, F. Behr, H. Barnert, Nucl. Eng. Des./Fusion 78 (1984) 285–291.
[5] A. Fujishima, K. Honda, Nature 238 (1972) 37–38.
[6] M.R. Hoffmann, S.T. Martin, W.Y. Choi, D.W. Bahnemann, Chem. Rev. 95 (1995) 69–96.
[7] A.L. Linsebigler, G.Q. Lu, J.T. Yates, Chem. Rev. 95 (1995) 735–758.
[8] A. Wold, Chem. Mater. 5 (1993) 280–283.
[9] R. Asahi, T. Morikawa, T. Ohwaki, K. Aoki, Y. Taga, Science 293 (2001) 269–271.
[10] R. Nakamura, T. Tanaka, Y. Nakato, J. Phys. Chem. B 108 (2004) 10617–10620.
[11] S. Goldstein, D. Behar, J. Rabani, J. Phys. Chem. C 112 (2008) 15134–15139.
[12] Y. Huang, W. Ho, S. Lee, L. Zhang, G. Li, J.C. Yu, Langmuir 24 (2008) 3510–3516.
[13] T. Umebayashi, T. Yamaki, S. Tanaka, K. Asai, Chem. Lett. 32 (2003) 330–331.
[14] N. Lu, X. Quan, J.Y. Li, S. Chen, H.T. Yu, G.H. Chen, J. Phys. Chem. C 111 (2007) 11836–11842.
[15] D. Li, H. Haneda, N.K. Labhsetwar, S. Hishita, N. Ohashi, Chem. Phys. Lett. 401 (2005) 579–584.
[16] H. Wang, J.P. Lewis, J. Phys. Condens. Matter. 18 (2006) 421–434.
[17] C. Di Valentin, G. Pacchioni, A. Selloni, Chem. Mater. 17 (2005) 6656–6665.
[18] S.U.M. Khan, M. Al-Shahry, W.B. Ingler Jr., Science 297 (2002) 2243–2245.
[19] K. Noworyta, J. Augustynski, Electrochem. Solid-State Lett. 7 (2004) E31–E33.
[20] C. Xu, S.U.M. Khan, Electrochem. Solid-State Lett. 10 (2007) B56–B59.
[21] C. Xu, Y.A. Shaban, W.B. Ingler Jr., S.U.M. Khan, Sol. Energy Mater. Sol. Cells 91 (2007) 938–943.
[22] C. Hagglund, M. Gratzel, B. Kasemo, Science 301 (2003) 1673b.
[23] A.B. Murphy, Sol. Energy Mater. Sol. Cells 92 (2008) 363–367.
[24] B. Neumann, P. bogdanoff, H. Tributsch, S. Sakthivel, H. Kisch, J. Phys. Chem. B 109 (2005) 16579–16586.
[25] C.S. Enache, J. Schoonman, R. van de Krol, J. Electroceram. 13 (2004) 177–182.
[26] L. Zhu, X.L. Cui, J. Shen, X.L. Yang, Z.J. Zhang, Acta Phys.: Chim. Sin. 23 (2007) 1662–1666.
[27] E. Gyorgy, G. Socol, E. Axente, I.N. Mihailescu, C. Ducu, S. Ciuca, Appl. Surf. Sci. 247 (2005) 429–433.
[28] T. Yoshida, Y. Fukami, M. Okoshi, N. Inoue, Jpn. J. Appl. Phys. 44 (2005) 3059–3062.
[29] T. Bak, J. Nowotny, M. Rekas, C.C. Sorrell, Int. J. Hydrogen Energy 27 (2002) 991–1022.
[30] G. Milczarek, A. Kasuya, S. Mamykin, T. Arai, K. Shinoda, K. Tohji, Int. J. Hydrogen Energy 28 (2003) 919–926.

[31] C.A. Grimes, O.K. Varghese, S. Ranjan, Light Water Hydrogen: The Solar Generation of Hydrogen by Water Photoelectrolysis, Springer Science/Business Media, New York, 2008.
[32] H.P. Klug, L.E. Alexander, X-ray Diffraction Procedures for Polycrystalline and Amorphous Materials, John Wiley & Sons, Inc., New York, 1959.
[33] E. Sanchez, T. Lopez, R. Gomez, Bokhimi, A. Morales, O. Novaro, J. Solid State Chem. 122 (1996) 309–314.
[34] I.E. Grey, C. Li, D.M. Macrae, L.A. Bursill, J Solid State Chem. 127 (1996) 240–247.
[35] D. Gonbeau, C. Guimon, G. Pfisterguillouzo, A. Levasseur, G. Meunier, R. Dormoy, Surf. Sci. 254 (1991) 81–89.
[36] M.E. Schulz, H. Lin, M. Day, S.I. Shah, Society of Vacuum Coaters Annual Technical Conference, SVC, 2009, CT-14.
[37] H. Lin, C.P. Huang, W. Li, C. Ni, S.I. Shah, Y.H. Tseng, Appl. Catal. B 68 (2006) 1–11.
[38] A.B. Murphy, Sol. Energy Mater. Sol. Cells 91 (2007) 1326–1337.
[39] K. Vinodgopal, S. t Hotchandani, P.V. Kamat, J. Phys. Chem. 97 (1993) 9040–9044.
[40] M. Takahashi, K. Tsukigi, T. Uchino, T. Yoko, Thin Solid Films 388 (2001) 231–236.
[41] H. Lin, A.K. Rumaiz, M. Schulz, D. Wang, R. Rock, C.P. Huang, S.I. Shah, Mater. Sci. Eng. B 151 (2008) 133–139.
[42] H. Park, C.D. Vecitis, M.R. Hoffmann, J. Phys. Chem. A 112 (2008) 7616–7626.
[43] Y.Z. Yang, C.H. Huang, H. Idriss, Appl. Catal. B 67 (2006) 217–222.
[44] O.K. Varghese, C.A. Grimes, Sol. Energy Mater. Sol. Cells 92 (2008) 374–384.